AGU PUBLICATIONS

JGR

Journal of Geophysical Research: Space Physics

RESEARCH ARTICLE
10.1002/2015JA021630

Key Points:
- First model result of dust layers at Mars
- First ionospheric result for different size of dust particles
- First comparison of equatorial *D* region ionosphere of Mars and Earth

Correspondence to:
S. A. Haider,
haider@prl.res.in

Citation:
Haider, S. A., I. S. Batista, M. A. Abdu, P. Muralikrishna, S. Y. Shah, and T. Kuroda (2015), Dust storm and electron density in the equatorial *D* region ionosphere of Mars: Comparison with Earth's ionosphere from rocket measurements in Brazil, *J. Geophys. Res. Space Physics*, *120*, 8968–8977, doi:10.1002/2015JA021630.

Received 29 JUN 2015
Accepted 22 SEP 2015
Accepted article online 28 SEP 2015
Published online 20 OCT 2015

Dust storm and electron density in the equatorial *D* region ionosphere of Mars: Comparison with Earth's ionosphere from rocket measurements in Brazil

S. A. Haider[1,2], I. S. Batista[1], M. A. Abdu[1], P. Muralikrishna[1], Siddhi Y. Shah[2], and T. Kuroda[3]

[1]Department of Aeronomy, Instituto Nacional de Pesquisas Espaciais, São Paulo, Brazil, [2]Space and Atmospheric Sciences, Physical Research Laboratory, Ahmedabad, India, [3]Department of Geophysics, Tohoku University, Sendai, Japan

Abstract We report the first model result for the dust densities and electron densities in the *D* region ionosphere of Mars for aerosol particles of different sizes during a major dust storm that occurred in Martian Year (MY) 25 at low latitude. These calculations are made at latitude 10°S and solar longitudes (Ls) = 200°, 220°, 250°, and 280° for high, medium, low, and absence of dust storms, respectively. Four corresponding dust layers were found at 50 km, 50 km, 38 km, and 25 km during these events. During high dust storm period, the optical depth and dust density increased by a factor of ~20 from its normal condition. The electron densities estimated for the *D* region ionosphere of Mars for submicron sized dust particles are largest as compared to that estimated for larger particles. The electron density reduced by ~2 orders of magnitude during high dust storm. The estimated electron density in the clear atmosphere of Mars is compared with measurements of Earth's ionosphere at nearly the same geophysical condition.

1. Introduction

A major dust storm was observed in Martian Year (MY) 25 by the Thermal Emission Spectrometer (TES) on board Mars Global Surveyor (MGS) during the spring season at southern low latitude between Ls = 180° and 300° that lasted a couple of weeks [*Smith et al*., 2013]. We have calculated the dust densities and the daytime electron densities in the spring season of MY25 between altitude 0 and 70 km at latitude 10°S and Ls = 200°, 220°, 250°, and 280° during high, medium, low, and the absence of dust storms corresponding to $\tau = 1.9$, 1.0, 0.5, and 0.1, respectively. The daytime ionosphere of Mars has not been observed at altitudes below 70 km [*Haider and Mahajan*, 2014]. The estimated results are compared with the electron density measured in the Earth's ionosphere under similar geophysical conditions.

During the last three decades several rockets carrying Langmuir Probe (LP) were launched from the Brazilian rocket launching sites in Natal (5.9°S, 35.2°W) and Alcantara (2.3°S, 44.4°W) to study the Earth's equatorial ionosphere [*Muralikrishna and Abdu*, 2006]. Three of them have measured electron densities in the *D* region ionosphere during late spring at solar zenith angles (SZA) ~ 94.5°, 102°, and 110°. One of them was launched from Alcantara on 23 November 2002 at local time 18:18. The other two rockets were launched on 2 December 2011 and 8 December 2012 at 19:00 LT from Alcantara and Natal, respectively.

The main objectives of this paper are (1) study of dust layers of different size of aerosol particles and their impact in the *D* region of equatorial ionosphere of Mars, (2) comparison of electron densities between *D* region ionospheres of Mars and Earth at similar geophysical conditions, and (3) study of the possible reasons for the deviations of the observed electron densities in the Earth's equatorial *D* region from the model values predicted for the *D* region ionosphere of Mars.

2. Dust Storms and Optical Depth Measurements

Thermal Emission Spectrometer (TES) and Thermal Emission Imaging System (THEMIS) on board MGS and Mars Odyssey have provided continuous observations of infrared dust optical depths, respectively, at wavelength 9.30 μm from MY24 to MY32 [*Montabone et al*., 2015]. These two experiments were intercalibrated by *Christensen et al*. [2003]. *Smith* [2004] gave an estimate for total uncertainty in TES absorption-only IR dust optical depth for the calibrated frame: 0.05 or 10% of the column optical depth, whichever is larger. *Smith* [2009] provided this value for THEMIS absorption-only IR dust optical depth for the calibrated frame: 0.04 or 10% of optical

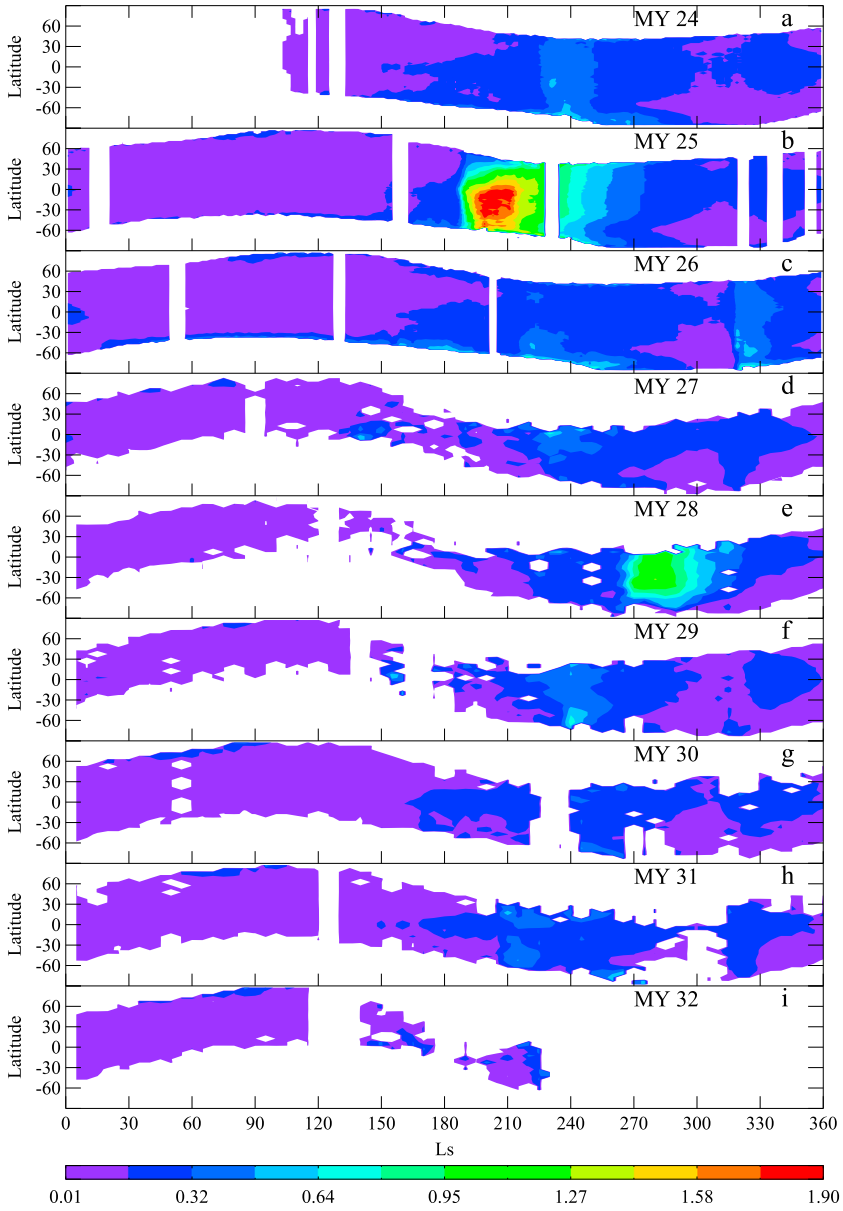

Figure 1. The dust optical depths obtained from MGS and Mars Odyssey observations for (a) MY24, (b) MY25, (c) MY26, (d) MY27, (e) MY28, (f) MY29, (g) MY30, (h) MY31, and (i) MY32.

depth, whichever is larger. MGS started its science mapping phase in March 1999 (Ls ~ 104°, MY24), after a long period of aerobraking. It stopped working in January 2007. Mars Odyssey started its mapping phase in February 2002 (Ls ~ 330°, MY25) and is still working. The dust optical depths as a function of latitude and Ls are plotted in Figures 1a–1i for nine Martian years between MY24 and MY32. Two dust storms were observed in MY25 and MY28 at southern low latitudes. In this figure, MGS data are plotted between MY24 (from Ls = 0°) and MY27 (till Ls = 81°) followed by Mars Odyssey data till MY32. MGS measured optical depths daily at 2:00 P.M. and 2:00 A.M. The local time of Mars Odyssey observation varies between 2:00 P.M. and 6:00 P.M. The morning observations are not used for dust retrieval. These data are averaged over longitudes. The Ls and latitude values refer to the center of 5° × 5° bins. In this paper, we have used optical depth of the first major dust storm that occurred at low latitude in the southern spring of MY25. During high dust storm period, the optical depths increased to about 1.9 at Ls = 200°. After a couple of days, the intensity of this dust storm reduces and the optical depth decreases to 1.0 at Ls = 220°, which we consider a medium dust storm. The effect of dust storm becomes very low with the optical depth ~0.5 at about Ls = 250°. This observation shows that the dust storm took 3 to

4 months for the dust to settle down to its normal condition. Very low optical depth ~0.1 is observed in the late spring at about Ls = 280°. We consider it a background aerosol loading in the clean atmosphere when dust storm is absent. These storm conditions refer to different periods of a single storm (Ls ~ 200°, MY25) and not defined by different storm intensities for several observed dust storms.

3. Model Calculation and Input Parameters

3.1. Dust Densities of Different Size of Aerosol Particles

We have calculated the surface density of the dust from the equation, $n_s \sim n_0(\tau/\tau_0)$, where n_s is the surface density of dust particles in cm^{-3}, τ is the measured optical depth taken from Figure 1b, τ_o is the background optical depth equal to 0.1 and n_o is the dust density equal to 2 cm^{-3} in the clean atmosphere [cf. *Montabone et al.*, 2015]. The altitude profiles of dust densities are calculated using the profile shape parameters determined from a recent observation made by Mars Climate Sounder (MCS) on board the Mars Reconnaissance Orbiter (MRO). These observations show an elevated maximum in the dust profiles above 20 km in most of the seasons of Southern Hemisphere [cf. *Heavens et al.*, 2014; *Guzewich et al.*, 2014]. Using the surface density of the dust (n_s), we have calculated height density profiles of dust particles from the following equations as given below

$$n(r,z) \sim k \cdot n_s \cdot n(r) \cdot A(z) \tag{1}$$

where $n(r)$ is the density distribution of aerosol particles of radius r, k is a constant, and $A(z)$ is a parameterized scheme at altitude z as given below

$$A(z) = \left[1 - \exp\left[-\frac{(z-\mathrm{FH})^2}{\mathrm{FL}^2}\right]\right] + B \cdot \exp\left[-\frac{(z-\mathrm{PH})^2}{\mathrm{PT}^2}\right] \tag{2}$$

The parameters FH (fall off height), FL (fall off length), PH (pulse height), PT (pulse thickness), and B (ratio of peak to surface dust) have been estimated from MCS observations [cf. *Heavens et al.*, 2014] and vary with season and latitude. B is a dimensionless parameter. The FH, PH, PT, and FL are given in km. We have used a dust density distribution, which was retrieved from the observations of TES experiment on board MGS. It is given by a modified Gamma distribution function [*Wolff et al.*, 2006] as follows:

$$n(r) = r^a \cdot \exp(-br) \tag{3}$$

where $a = (1 - 3v_{\mathrm{eff}})/v_{\mathrm{eff}}$ and $b = 1/(v_{\mathrm{eff}} \cdot r_{\mathrm{eff}})$. The a and b are adjustable parameters, which control size and width of the Gamma distribution. The terms r_{eff} and v_{eff} are the effective radius and effective variance (width), respectively. The effective radius and effective variance are defined as [*Hansen and Travis*, 1974]

$$r_{\mathrm{eff}} = \frac{\int_{r_1}^{r_2} r^2 \; n(r)\, r\, \mathrm{d}r}{\int_{r_1}^{r_2} r^2 \; n(r)\, \mathrm{d}r} \tag{4}$$

$$v_{\mathrm{eff}} = \frac{\int_{r_1}^{r_2} (r - r_{\mathrm{eff}})^2 r^2 \; n(r)\, \mathrm{d}r}{r_{\mathrm{eff}}^2 \int_{r_1}^{r_2} r^2 \; n(r)\, \mathrm{d}r} \tag{5}$$

where r_{eff}^2 in the denominator makes v_{eff} dimensionless, $r_1 = 0$ and $r_2 = \infty$. Using equations (3) to (5), we can obtain $r_{\mathrm{eff}} = a$, $v_{\mathrm{eff}} = \mathrm{b}$. Values of r_{eff} and v_{eff} are changing for different aerosols. Therefore, the dust density will be different for different values of r_{eff} and v_{eff}. In our model, we have used values of r_{eff} and v_{eff} equal to 1.8 μm and 0.3, respectively. These values are representative for conditions sampled by the Compact Reconnaissance Imaging Spectrometer (CRISM) on board MRO [*Wolff et al.*, 2009].

The minimum sizes of dust and water ice aerosols were observed to be ~0.2 and 0.1 μm, respectively, from CRISM observations [cf. *Smith et al.*, 2013; *Guzewich et al.*, 2014]. The densities of dust aerosols are very low at all altitudes for the radius greater than 3 μm. Therefore, we have calculated size distribution of dust aerosols between 0.2 and 3 μm. The constant $k = 1/\left(\int_0^\infty n(r)\mathrm{d}r\right)$ is obtained by integrating $n(r)$ from r to $r + \mathrm{d}r$. *Guzewich et al.* [2014] have

reported that the size of the dust particle is constant with respect to height in almost all seasons of Southern Hemisphere. We therefore assume the same value of r_{eff} at all altitudes. Using equations (1)–(5), we have calculated altitude profiles of dust densities at latitude 10°S for six different size of aerosol particles of radius $r = 0.2$, 0.6, 1.0, 1.4, 2.0, and 3.0 μm. These dust concentrations are used in the ion-dust chemical model [*Haider et al*., 2010] to calculate the electron densities in the *D* region ionosphere of Mars.

3.2. Electron Densities for Different Sizes of Aerosol Particles

Galactic cosmic rays (GCR) are the main source for the formation of the *D* layer in the Martian ionosphere [*Haider and Mahajan*, 2014]. Recently, Radiation Assessment Detector (RAD) on board Mars Science Laboratory's Curiosity rover has measured the energetic particle radiation environment on the surface of Mars [*Ehresmann et al*., 2014]. GCR consists of 87% protons, 12% helium, and 1% heavier nuclei. The impact of primary GCR on to the atmospheric molecules produces protons, neutrons, and pions. Fast secondary nucleons can gain enough energy to increase the production of the particles by neutral collisions. Neutral pions quickly decay to gamma rays, and their contribution to the energy deposition is very important in the lower part of the atmosphere. At high altitudes (~30 to 50 km), the maximum ion production rates are due to protons. The charged pions decay to muons, which do not decay before reaching the ground; and hence, the muon energy is mainly observed by RAD experiment on the Martian surface.

Recently, *Haider et al*. [2010] have developed an ion-dust aerosol model for the calculation of the electron density in the lower ionosphere of Mars. We have extended this model to study the characteristics of dust storms of different size of aerosol particles and their influence in the *D* region ionosphere of Mars. In this model, energy loss method and continuity equations were combined together. The energy loss method calculates ion production rates of various atmospheric gases by GCR ionization. The production rates for different size of charged aerosols are calculated by the product of ion-aerosol attachment coefficient with the densities of dust and atmospheric ions. The dust densities of different size of aerosol particles are calculated from equation (1). These production rates are used in the continuity equations, which calculate the electron density. In this model, ion-dust chemical scheme is taken from *Haider et al*. [2010]. The temperature and neutral atmosphere used in this model are shown in Figure 2. Using this model, we have calculated electron densities for six different sizes of aerosol particles of radius 0.2, 0.6, 1.0, 1.4, 2.0, and 3.0 μm due to absorption of GCR at SZA 75°. The flux of incident GCR is exponentially attenuated and is calculated between values 10^3 to 10^{-5} particles $m^{-2}\,s^{-1}\,GeV^{-1}\,Ster^{-1}$ at energy interval 1 to 1000 GeV [cf. *Haider et al*., 2010].

3.3. Mixing Ratio, Temperature, and Neutral Density Model Used

We have used a model atmosphere of dust and eight atmospheric gases (CO_2, N_2, Ar, O, O_2, CO, H_2O, and O_3). Figures 2a–2d represent the altitude profiles of mixing ratios of these gases in spring season of MY25 at latitude 10°S and Ls = 200°, 220°, 250°, and 280°, respectively. These data are taken from Mars Climate Database (MCD) [*Millour et al*., 2014] (website: http://www-mars.lmd.jussieu.fr). The N_2, Ar, and O_2 are noncondensable gases. The condensations of CO_2 and CO are negligible heat sources at the equator [*Millour et al*., 2014]. Only in the polar region do CO_2 and CO condensations have significance. Therefore, the mixing ratios of five gases CO_2, N_2, O_2, Ar, and CO are nearly constant with altitude, close to the equator. Unlike these major gases, the mixing ratios of trace gases H_2O, O_3, and O are changing with altitude. The mixing ratio of H_2O shows a small layer between altitude 20 and 40 km during spring season at low latitudes in Southern Hemisphere. This layer may be produced due to the following two reasons.

1. Solar heating is largest near the equator in Mars. The Hadley circulation transports water vapor from ~30°N to 30°S latitude in Mars [cf. *Millour et al*., 2014]. This circulation may be pumping the H_2O high into the atmosphere near the equator altering its mixing ratio.
2. Mars has experienced a dust storm in MY25 during spring season (Ls ≈ 200°–250°) at low latitudes of the Southern Hemisphere. During high dust storm period at Ls = 200°, dust opacity raises the air temperature by up to 50 K between altitudes 30 and 40 km from its normal condition (see Figure 2f). At high temperature, CO_2 sublimates between spring and summer seasons leaving traces of water, therefore increasing the mixing ratio of water vapor.

The mixing ratio of O is significantly low below 25 km because atomic oxygen is destroyed by water vapor in this altitude region. Above 25 km, H_2O condensation is very small; therefore, the mixing ratio of O is increasing rapidly with height. The O_3 is preferentially created from three body reaction due to combination of O, O_2, and CO_2, where

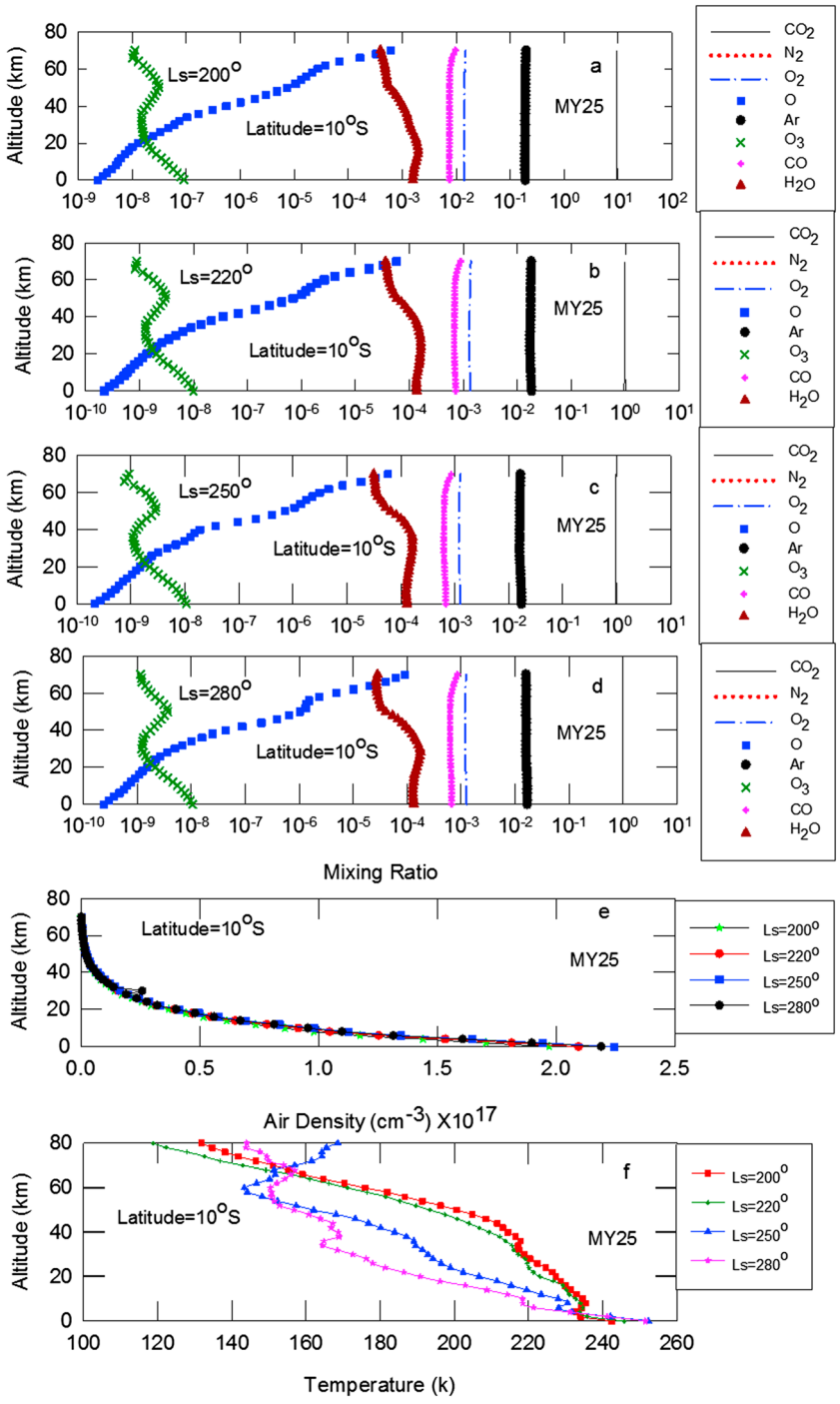

Figure 2. Altitude profiles of mixing ratios of eight atmospheric gases at latitude 10°S for spring season of MY25 at (a) Ls = 200°, (b) Ls = 220°, (c) Ls = 250°, and (d) Ls = 280° with (e) air densities and (f) temperatures. The mixing ratios of N_2 and Ar are nearly same.

the densities are high (i.e., near the surface of Mars). At high altitudes, production of O_3 decreases with the density and the balance between O and O_3 move toward O from the photolysis of O_3 ($O_3 + h\nu \rightarrow O + O_2$). This process decreases O_3 at high altitude. There is a distinct peak in the mixing ratio of O_3 at about 50 km. This peak is formed when loss of O_3 is low by HO_x radical due to lack of H_2O in that region [*Lefevre et al.*, 2004; *Lebonnois et al.*, 2006] The air densities and temperatures at latitude 10°S during spring

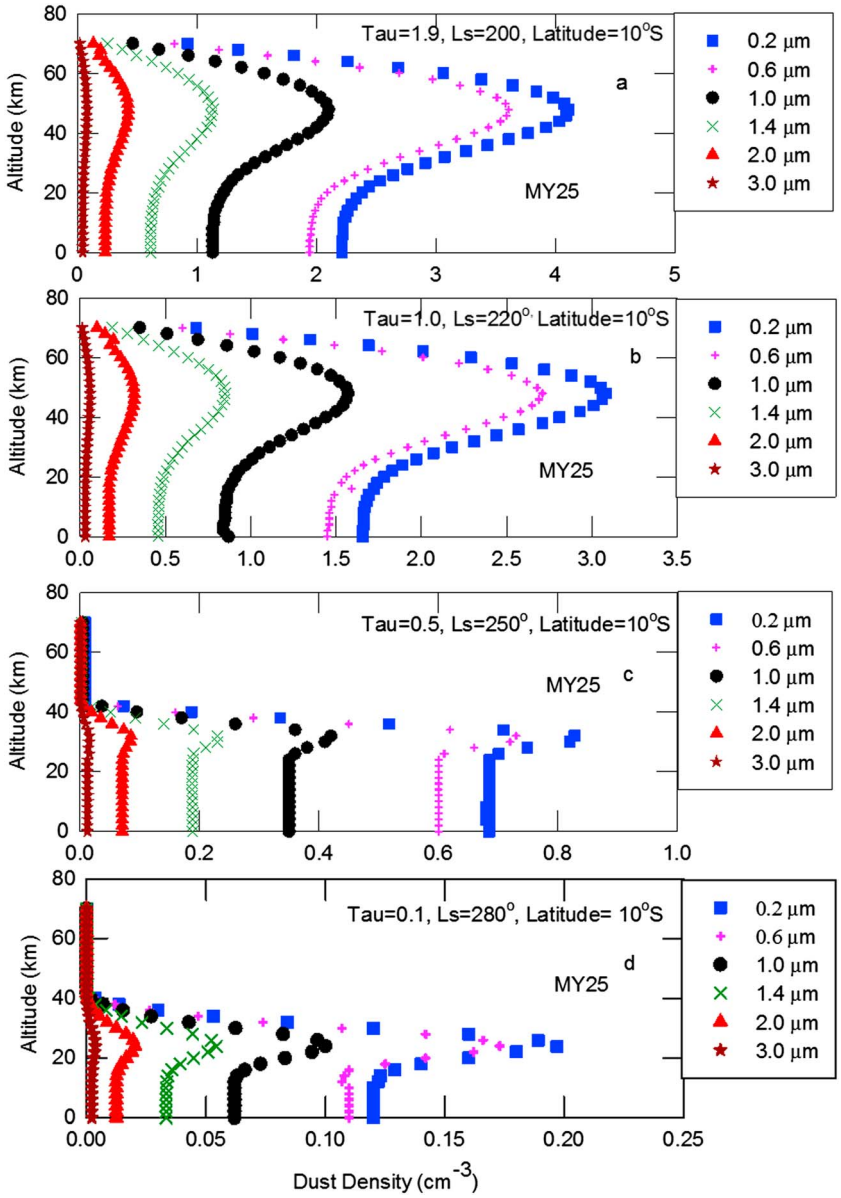

Figure 3. Altitude profiles of dust densities at 10°S for different size of aerosol particles in the spring season of MY25 at (a) Ls = 200°, (b) Ls = 220°, (c) Ls = 250°, and (d) Ls = 280°.

season of MY25 at Ls = 200°, 220°, 250°, and 280° are shown in Figures 2e and 2f, respectively. Based on MGS measurements in MY25, the low dust storm at Ls = 250° for $\tau = 0.5$ is confined to altitude region ~ 25–30 km, while medium and high dust storms at $L = 220°$ and Ls = 200° for $\tau = 1.0$ and 1.9, respectively, have risen to altitude ~ 50 km (see Figures 3a–3c). The dust storm is transported from the surface to about 70 km through dynamical coupling processes providing expansion of the lower atmosphere, which increased the densities and temperature during this event. In Figures 2e and 2f, air densities and temperatures are calculated from global circulation model [*Kuroda et al.*, 2005] during spring season of MY25 at latitude 10°S and Ls = 200°, 220°, 250°, and 280° for high, medium, low, and the absence of dust storm, respectively. The mixing ratios of CO_2, N_2, O_2, O, H_2O, O_2, CO, and Ar are multiplied by the air density to obtain the neutral density model atmosphere of Mars. Since the dust opacities are zonally averaged over longitudes (see Figure 1), we have also averaged mixing ratios, air densities, and temperatures over longitude. It should be noted that air densities/temperatures in the lower atmosphere at low latitude are not changing significantly with longitude.

4. Results and Discussion

4.1. Dust Layers in the *D* Region Ionosphere of Mars

Figures 3a–3d represent the concentration profiles of dust aerosol of size 0.2, 0.6, 1.0, 1.4, 2.0, and 3.0 μm in spring season of MY25 at latitude 10°S and Ls = 200°, 220°, 250°, and 280° for high dust storm ($\tau = 1.9$), medium dust storm ($\tau = 1.0$), low dust storm ($\tau = 0.5$), and the absence of dust storm ($\tau = 0.1$), respectively. The concentrations of dust aerosols of size > 3 μm are nearly zero in the lower atmosphere of Mars. We have considered that background optical depth is equal to 0.1 when the atmosphere is clean from the dust loading. Thus, aerosol particles of $\tau = 0.1$ are present in the clean atmosphere during the absence of dust storm. It is found that the dust density is high for smaller sized particles. Since the gravitation settling velocity is directly proportional to the size (and therefore mass) of aerosol particles, the larger particles settle down quickly and their concentrations are lower than the small particles. We have found that the small dust particle of size 0.2 μm produces peak densities ~ 4.2 cm^{-3}, 3.2 cm^{-3}, 0.8 cm^{-3}, and 0.2 cm^{-3} at 50 km, 50 km, 38 km, and 25 km during high, medium, low, and the absence of dust storms, respectively. Recently, *Guzewich et al*. [2014] and *Heavens et al*. [2014] have studied vertical distribution of dust aerosol for the same dust storm conditions in the dayside tropical atmosphere of Mars. They have found two distinct layers in the dust profiles, one at altitude ~ 20–30 km and other at altitude ~ 45–65 km from the observations by CRISM and MCS experiments, respectively. Our estimated profiles of dust densities are consistent with the dust layers observed by CRISM and MCS experiments, which produces an elevated maximum in the *D* region ionosphere of Mars.

4.2. Comparison of *D* Region Electron Density of Earth and Mars' Ionosphere

Before comparison between *D* region ionosphere of Earth and Mars, it would be useful to recall some of the more salient characteristics of these planets that affect the electron density.

1. The mean atmospheric pressures on Mars and on Earth are 6 mbar and 1000 mbar, respectively. Therefore, GCR can penetrate deeper into the atmosphere of Mars as compared to its penetration depth on Earth's atmosphere.
2. The *D* region ionosphere of Mars is highly influenced by dust storms, which are rarely observed on Earth.
3. The low-latitude ionosphere of Earth is influenced by electrodynamics processes, which are not important in the Martian ionosphere because electric and magnetic fields are not intense enough on Mars as they are on Earth.
4. In the *D* region ionosphere where most of the energies of GCR are absorbed, the atmosphere consists largely of CO_2 on Mars and of N_2 and O_2 on Earth. Most of these characteristics are subject to substantial variations, which should be taken into consideration in a detailed comparison of the *D* region electron density of these planets. Such a comparison is beyond the scope of this study, but we will compare our model calculation of Mars ionosphere with the specific electron density of Earth's ionosphere pertaining to nearly similar physical conditions.

Figures 4a–4d represent electron density profiles in the *D* region ionosphere of Mars for dust aerosol of sizes 0.2, 0.6, 1.0, 1.4, 2.0, and 3.0 μm at latitude 10−S during spring season of MY25 at Ls = 200°, 220°, 250°, and 280° for high, medium, low, and the absence of dust storms, respectively. The electron densities are decreasing with increasing size of dust particles, that is with increasing dust optical depths. The small dust particles can attach easily to atmospheric ions. Therefore, electron densities are produced more in the *D* region ionosphere of Mars for dust particles of minimum size 0.2 μm. The attachment of dust to atmospheric ions is a sink process, which reduces peak electron densities in the *D* region ionosphere of Mars by ~ 2 orders of magnitude during dust storm. The value of $\tau = 0.1$ is assumed a threshold optical depth above which perturbation due to dust storm in the *D* region ionosphere of Mars is significant.

The electron density in the clean atmosphere ($\tau = 0.1$ and $r = 0.2$ μm) of Mars is compared with the *D* region electron density on the Earth's ionosphere. The *D* region electron densities have been observed in the Earth's ionosphere at altitude range ~ 60–90 km due to impact of GCR and solar Lyman alpha radiation [cf. *Haider and Mahajan*, 2014]. GCR is a major ionization source at the lower height limit of the Earth's ionosphere. Lyman α ionizes NO above 75 km where its density is larger in the Earth's ionosphere by 2–3 orders of magnitude as compared to that observed in the Martian atmosphere. The surface concentration of CO_2 on Mars is about 70 times smaller than the surface concentration of N_2 and O_2 on Earth. Therefore, GCR penetrate deeper into Martian atmosphere to form a permanent *D* layer at altitude ~34 km, which is lower in altitude as compared to that observed in the Earth's ionosphere, where the main source of ionization is solar Lyman α radiation.

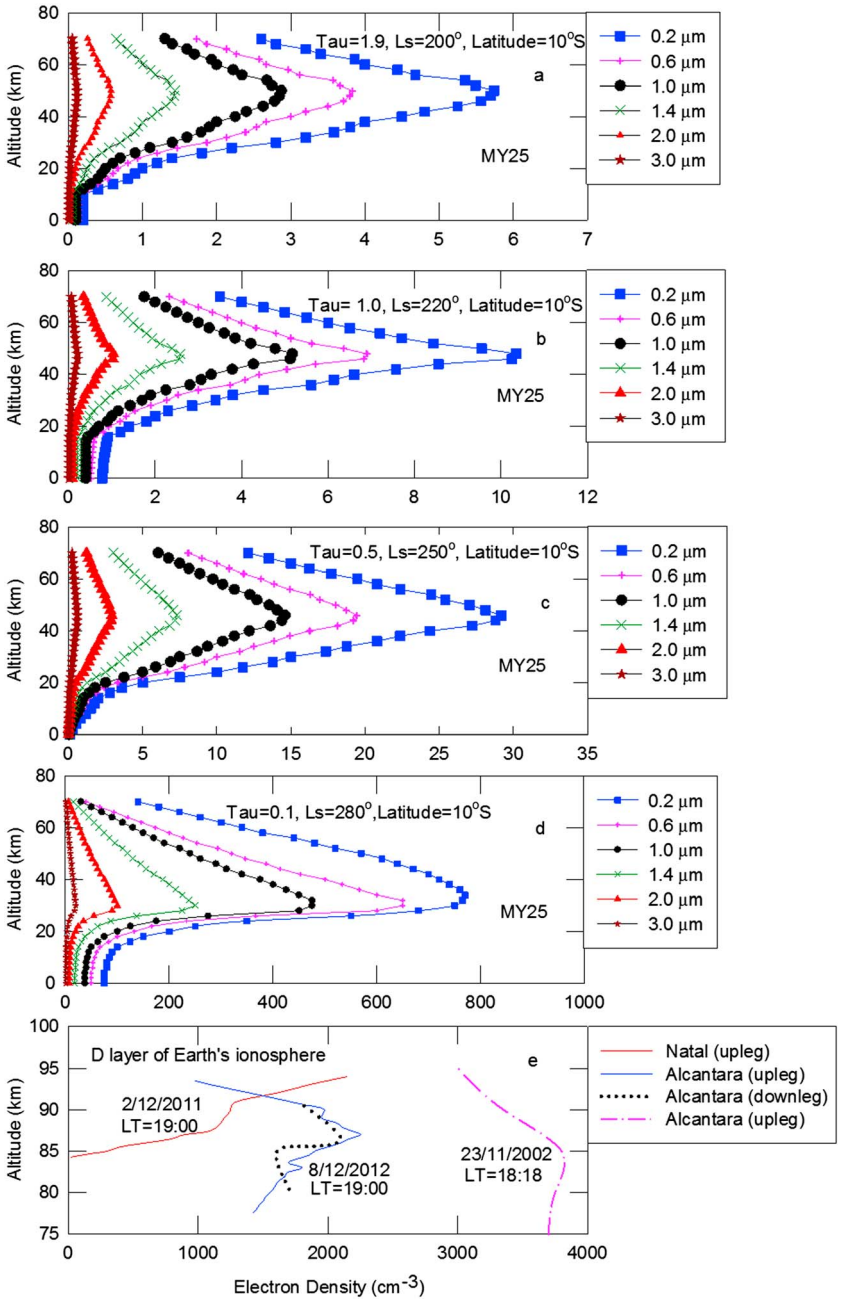

Figure 4. Altitude profiles of electron densities at latitude 10°S for different size of aerosol particles in the spring season of MY25 at (a) Ls = 200°, (b) Ls = 220°, (c) Ls = 250°, and (d) Ls = 280°. (e) Rocket measurements of Earth's ionosphere in the *D* region from Brazil for comparison with Mars' ionosphere.

Figure 4e represents electron density profiles from three measurements carried out in late spring (close to late spring season on Mars at Ls = 280°) from LP experiment on board Brazilian Sonda 3 rockets, flown in the evening from Natal (5.9°S, 35.2°W) and Alcantara (2.3°S, 44.4°W) launch sites on 23 November 2002, 2 December 2011, and 8 December 2012, respectively. Both the upleg and downleg profiles are shown for the 8 December flight. The electron densities measured on 23 November 2002 are larger by a factor of 2–3 than those observed on 2 December 2011 and 8 December 2012. This is due to the fact that it was made at an earlier local time. These measurements were made at different solar cycle epochs. The first of these measurements from Alcantara in 2002 was carried out in solar cycle 23 of solar maximum condition. The second and third measurements from Natal and Alcantara were made in 2011 and 2012, respectively, during

Table 1a. Properties of *D* Region Electron Density on Earth

Date	Peak Density (cm^{-3})	Peak Height (km)	Location	Solar Activity	SZA	Season	Local Time (h)	Lyman α Flux ($m^{-2}s^{-1}$)
2/12/2011 (upleg)	1.3×10^3	Layer ~ 88	Natal (5.9°S, 35.2°W)	Medium	110°	Late Spring	19:00	4.56×10^{15}
8/12/2012 (upleg)	2.4×10^3	86	Alcantara (2.3°S, 44.4°W)	Medium	102°	Late Spring	19:00	4.24×10^{15}
23/11/2002 (upleg)	3.8×10^3	84	Alcantara (2.3°S, 44.4°W)	Maximum	94.5°	Late Spring	18:18	4.96×10^{15}
8/12/2012 (downleg)	2.1×10^3	85	Alcantara (2.3°S, 44.4°W)	Medium	102°	Late Spring	19:00	4.24×10^{15}

solar cycle 24 of lower solar flux (solar medium) condition. The solar Lyman α radiation is a major driver of *D* region electron density on the dayside ionosphere of Earth. It is observed to be 4.56×10^{15}, 4.24×10^{15}, and 4.96×10^{15} photons $m^{-2}s^{-1}$ on 2 December 2011, 8 December 2012, and 23 November 2002, respectively (http://lasp.colorado.edu/lisird/lya/). There is no significant difference in the electron density profiles obtained on 8 December 2012 during the upleg and downleg trajectory of rocket. The downleg electron density was not observed on 23 November 2002 in the *D* region ionosphere of Earth. Because of a large error found in the downleg electron density measurements on 2 December 2011, we do not report it. We may note three distinct electron density peaks ~ 3.8×10^3 cm^{-3}, 2.1×10^3 cm^{-3}, and 2.4×10^3 cm^{-3} at altitudes 84 km, 85 km, and 86 km, respectively, during two rocket flights conducted from Alcantara on 23 November 2002 and 8 December 2012, respectively. This peak is not clearly seen in the electron density profile measured over Natal on 2 December 2011. However, in the same altitude region, a small layer with the electron density ~ 1.3×10^3 cm^{-3} can be noticed. This value is to be compared with the peak electron density estimated in the clean atmosphere ($\tau = 0.1$ and $r = 0.2$ μm) of Mars. However, the peak electron density measured on 23 November 2002 from Alcantara in the *D* region of Earth's ionosphere is larger by factor of 5 and 2.5, respectively, than that estimated in the *D* region ionosphere of Mars for clean atmospheric condition.

The properties of *D* region electron densities of Earth's ionosphere are compared with the estimated electron densities in the clear atmosphere of Mars in Tables 1a and 1b, respectively. Tables 1a and 1b represent a summary of measurement dates, peak densities, peak heights, locations, solar cycles, SZA, seasons, local time, and Lyman α/GCR flux considered for *D* region electron densities of Earth's and Mars ionosphere. In Table 1a, SZA is calculated from the local times of the measurements using the formula given by *Querino et al.* [2006]. Since Ls is the Mars-Sun angle, it cannot be given in Table 1a for the dates of rocket measurements. However, period of spring season in Southern Hemisphere of Earth and Mars can be represented between Ls = 180° and 270° on the basis of equinoxes and solstices of both planets. Under same equinox/solstice conditions, late southern spring season on Mars occurred at Ls = 280°, which is very close to the month of November/December in Brazil. In Table 1b, peak densities, peak heights, location, SZA, Ls, and GCR flux are taken from model calculation. The dates are converted into Earth's year for MY25. The local time is converted as SZA 15° = 1 h, then SZA = 75° = 17:00 h based on MCD [*Millour et al.*, 2014]. It should be noted that measurements on Earth and Mars were not carried in the same year. This is because of the fact that rocket observations are very limited. We have compared all the measurements carried out in the *D* region ionosphere of Earth with the model calculations of *D* region ionosphere of Mars at nearly the same physical conditions.

5. Conclusion

The dust densities and electron densities due to different sizes of aerosol particles are estimated at latitude 10°S in the *D* region ionosphere of Mars during a major dust storm in spring season of MY25. In this dust storm, the optical depth and dust density increased by a factor of ~ 20, while the electron density decreased by ~ 2 orders of magnitude for several weeks until it settled down to its normal condition. The dust densities

Table 1b. Properties of *D* Region Electron Density in the Clear Atmosphere of Mars

Date	Peak Density (cm^{-3})	Peak Height (km)	Location	Solar Activity	SZA	Ls	Local Time (h)	GCR Flux ($m^{-2}s^{-1}GeV^{-1}ster^{-1}$)
22/07/2001	5.7	50	10°S	Maximum	75°	200°	17:00	10^3–10^{-5}
24/08/2001	10.4	48	10°S	Maximum	75°	220°	17:00	10^3–10^{-5}
10/10/2001	29.2	46	10°S	Maximum	75°	250°	17:00	10^3–10^{-5}
27/11/2001	770.0	34	10°S	Maximum	75°	280°	17:00	10^3–10^{-5}

represent four distinct layers at altitudes 50 km, 50 km, 38 km, and 25 km during the spring season at Ls = 200°, 220°, 250°, and 280°, respectively. In comparing *D* region ionosphere of Mars with Earth's ionosphere, we have considered the electron density peak estimated in the clear atmosphere ($\tau = 0.1$ and $r = 0.2\ \mu$m) of Mars as being suitable for comparison with the rocket measurements on Earth. However, the estimated peak densities in dusty atmosphere of Mars are lower by factors of 2–5 from the measurements on Earth. The peak heights of calculated electron densities on Mars are lower by a factor of 3 with respect to the measurements on the Earth. The comparative study of *D* region ionospheres of Earth and Mars is important to understand the physical, chemical, and dynamical processes in the lower ionospheres of both planets.

Acknowledgments
Authors are thankful to MGS and Mars Odyssey data team and M.D. Smith (Michael.d.smith@nasa.gov) for providing the data for this work. Authors also acknowledge MCD team of E. Millour (ehouarn.millour@lmd.jussieu.fr) for providing freely accessible Mars Climate Data (http://www-mars.lmd.jussieu.fr). One of the authors, S.A. Haider, also thanks FAPESP for support through visiting scientist fellowship by the process 2014/2199S-3 to work at INPE, Brazil.

Michael Liemohn thanks two reviewers for their assistance in evaluating this paper.

References

Christensen, P. R., et al. (2003), Miniature Thermal Emission Spectrometer for the Mars exploration rovers, *J. Geophys. Res.*, *108*(E12), 8064, doi:10.1029/2003JE002117.

Ehresmann, B., et al. (2014), Charged particle spectra obtained with Mars Science Laboratory Radiation Assessment Detector (MSL/RAD) on the surface of Mars, *J. Geophys. Res. Planets*, *119*, 468–479, doi:10.1002/2013JE004547.

Guzewich, S. D., M. D. Smith, and M. J. Wolff (2014), The vertical distribution of Martian aerosol particle size, *J. Geophys. Res. Planets*, *119*, 2694–2708, doi:10.1002/2014JE004704.

Haider, S. A., and K. K. Mahajan (2014), Lower and upper ionosphere of Mars, *Space Sci. Rev.*, *182*, 19–84.

Haider, S. A., V. Sheel, M. D. Smith, W. C. Maguire, and G. J. Molina-Cuberos (2010), Effect of dust storms on the *D* region of the Martian ionosphere: Atmospheric electricity, *J. Geophys. Res.*, *115*, A12336, doi:10.1029/2010JA016125.

Hansen, J. E., and L. D. Travis (1974), Light scattering in planetary atmospheres, *Space Sci. Rev.*, *16*, 527–610.

Heavens, N. G., M. S. Johnson, W. A. Abdou, D. M. Kass, A. Kleinböhl, D. J. McCleese, J. H. Shirley, and R. J. Wilson (2014), Seasonal and diurnal variability of detached dust layers in the tropical Martian atmosphere, *J. Geophys. Res. Planets*, *119*, 1748–1774, doi:10.1002/2014JE004619.

Kuroda, T., N. Hashimoto, D. Sakai, and M. Takahashi (2005), Simulation of the Martian atmosphere using a CCSR/NIES AGCM, *J. Meteorol. Soc. Jpn.*, *83*, 1–9.

Lebonnois, S., E. Quémerais, F. Montmessin, F. Lefèvre, S. Perrier, J.-L. Bertaux, and F. Forget (2006), Vertical distribution of ozone on Mars as measured by SPICAM/Mars Express using stellar occultations, *J. Geophys. Res.*, *111*, E09S05, doi:10.1029/2005JE002643.

Lefevre, F., S. Lebonnois, F. Montmessin, and F. Forget (2004), Three-dimensional modeling of ozone on Mars, *J. Geophys. Res.*, *109*, E07004, doi:10.1029/2004JE002268.

Millour, E., et al. (2014), A new Mars Climate Database v5.1, *The Fifth International Workshop on Mars Atmosphere: Modeling and Observations*, Oxford, U. K.

Montabone, L., et al. (2015), Eight-year climatology of dust optical depth on Mars, *Icarus*, *251*, 65–95, doi:10.1016/j.icarus.2014.12.034.

Muralikrishna, P., and M. A. Abdu (2006), Rocket measurements of ionospheric electron density from Brazil in the last two decades, *Adv. Space Res.*, *37*, 1091–1096.

Querino, C. A. S., M. A. N. Moura, R. F. D. F. Lyra, and e. G. L. Mariano (2006), Evaluate and comparison of global solar radiation and albedo with zenith angle in the Amazonic region, *Braz. J. Meteorol.*, *21*(3a), 42–49.

Smith, M. D. (2004), Interannual variability in TES atmospheric observations of Mars during 1999–2003, *Icarus*, *167*, 148–165.

Smith, M. D. (2009), THEMIS observations of Mars aerosol optical depth from 2002–2008, *Icarus*, *202*, 444–452, doi:10.1016/j.icarus.2009.03.027.

Smith, M. D., M. J. Wolff, R. T. Clancy, A. Kleinböhl, and S. L. Murchie (2013), Vertical distribution of dust and water ice aerosols from CRISM limb-geometry observations, *J. Geophys. Res. Atmos.*, *118*, 321–334, doi:10.1002/jgre.20047.

Wolff, M. J., et al. (2006), Constraints on dust aerosols from the Mars Exploration Rovers using MGS over flights and Mini-TES, *J. Geophys. Res.*, *111*, E12S17, doi:10.1029/2006JE002786.

Wolff, M. J., M. D. Smith, R. T. Clancy, R. Arvidson, M. Kahre, F. Seelos, S. Murchie, and H. Savijärvi (2009), Wavelength dependence of dust aerosol single scattering albedo as observed by the Compact Reconnaissance Imaging Spectrometer, *J. Geophys. Res.*, *114*, E00D04, doi:10.1029/2009JE003350.